Hindawi
Advances in Civil Engineering
Volume 2020, Article ID 1647197, 12 pages
https://doi.org/10.1155/2020/1647197

Research Article

Estimating the Uplift Bearing Capacity of Belled Piers Adjacent to Sloping Ground by Numerical Modeling Based on Field Tests

Yangchun Han,[1] Jiulong Cheng,[1] Weifeng Zheng,[2] and Shijun Ding[2]

[1]*College of Geoscience and Surveying Engineering, China University of Mining and Technology (Beijing), Beijing 100083, China*
[2]*Liangxiang Branch Institute, China Electric Power Research Institute, Beijing 102401, China*

Correspondence should be addressed to Jiulong Cheng; jlcheng@cumtb.edu.cn

Received 31 July 2019; Accepted 31 December 2019; Published 25 January 2020

Academic Editor: Jorge Branco

In order to evaluate the uplift bearing capacity of belled piers beside slopes, a series of numerical simulations are carried out based on field tests data. First, a number of uplift loading tests of full-scale belled piers are carried out on the project site of transmission line in Anhui Province, China. Second, a slope-foundation model for numerical modeling is proposed and calibrated based on field tests data. The behavior of belled piers adjacent to slopes subject to uplift load is studied by numerical modeling. The impact of three parameters, including distance (a) from the belled pier to the crest of the slope, slope angle (β), and embedment depth (h) of the belled pier, has been investigated on the uplift capacity of the belled pier. Based on the simulation results, an attenuation coefficient (ω) is put forward for evaluating the reduction of uplift bearing capacity of the belled pier. The results show that the coefficient ω is negatively correlated with distance a and depth h, and the influence of distance a is greater than that of depth h according to the results of variance analysis, but the difference is not significant by F test. Moreover, the empirical equation between attenuation coefficient ω and three key factors a, β, and h had been presented by a series of fitting.

1. Introduction

The rapid development of national economy puts forward higher demand for the construction of transmission lines. When the lines pass through mountainous and hilly areas, the foundations of line towers must be built at or near a sloping ground [1]. In either case, the existence of slopes may cause the attenuation of load-bearing capacity of foundations. The usual engineering solution is to increase the depth of the foundation while keeping the foundation as far away from the sloping ground as possible. However, due to the constraints of site topographic conditions and engineering costs, scientific analysis should be done to ensure the implementation of these measures. Therefore, it is of great significance to investigate the effect of slopes on the bearing capacity of adjacent foundations.

Many theoretical, numerical, and experimental results have been proposed to determine the load-bearing capacity of the footings adjacent to slopes or resting on slope surfaces [2–9]. Based on the results of slope model footing tests, Castelli and Lentini [2, 10] studied the influence of the slope distance on the bearing capacity of the foundation and determined the modified bearing capacity factors. However, most of the literatures mentioned above focus on the compressive performance of foundations, and only a few focuses on the uplift or lateral bearing capacity of the foundations embedded in sloping ground. Jiang et al. [11] studied the behavior of piles in sloping ground under undrained lateral loading conditions by finite element analysis. In addition, the representative field tests were completed by Lu et al. [12] and Qian et al. [13]. Based on two full-scale uplift load tests conducted on belled piers in the arid loess sloping ground, Lu et al. discussed the uplift resistance of foundation on slope from the characteristics of load-displacement curve, failure mode of soil, and ultimate uplift load. Similarly, based on the comparative in situ load test results of two types of foundations under combined uplift and lateral loads on a slope, Qian et al. analyzed the uplift and lateral bearing capacity of the foundations. The foundations studied by these two scholars are constructed on the

sloping ground, without considering the situation when the foundations are embedded near the slopes, which is inevitable in the process of tower foundation construction. Generally, increasing the distance between the foundation and the slope or embedding depth can increase the uplift resistance to match the unabated bearing capacity of the foundations that are far from slopes. And there are many qualitative analyses in this regard despite few quantitative ones.

The engineering background of this paper is a 220 kV transmission line which will pass through the mountainous and hilly areas in southern Anhui Province, China. It is necessary to evaluate the influence of slopes on the bearing capacity of foundations. However, the field tests of bearing capacity were carried out only on the foundations embedded in horizontal ground far from slopes instead of on the belled piers embedded near sloping ground for various reasons. Therefore, according to field test data, the numerical simulations were performed to evaluate the uplift bearing capacity of belled piers near slopes in this area. At the beginning of this research, five belled piers were tested under axial uplift load on a flat ground far from slopes. Based on the data of field tests, a 3D slope-foundation model was developed, calibrated, and validated. The uplift performance of belled piers adjacent to sloping ground was simulated using the model. The simulation results were analyzed, and the attenuation coefficient ω was taken as the index to quantitatively evaluate the uplift resistance of belled pier from three aspects: the distance a between belled pier and slope, the embedment depth h of the belled pier, and the slope angle β. These results will provide sufficient theoretical and data support for the construction of transmission line foundation in mountainous and hilly areas.

2. Experimental Study

In this section, the field tests of five full-scale belled piers under uplift loading are described. First of all, in order to determine the types and geomechanical properties of rock samples in the test area, a series of in situ tests and laboratory tests were carried out. Subsequently, the pouring and maintenance process of reinforced concrete foundation in site and the method and process of the loading test are illustrated. Finally, four commonly used failure criteria are introduced. One of them is selected through comparison to determine the ultimate uplift bearing capacity of foundation.

2.1. Test Site and Test Description. The field tests were carried out at a site along the 220 kV Huizhou–Wannan transmission line in Anhui Province, China. According to the preliminary investigation results of the project, the total length of the line is 35 km, with 91% in the mountains and 9% in the hills, respectively. Hence, the tower foundations of this line are mostly embedded in or near sloping ground. It is of great practical value to study the influence of slopes on bearing characteristics of adjacent foundations.

To determine the rock properties of the test site, a series of laboratory and in situ tests were performed according to relevant standards [14–18], including rock identification, microstructure, moisture content, specific gravity, point loading test, and shear strength measurements. The test results are listed in Table 1. Rock samples from the test site are eventually identified as strongly weathered lithic quartz complex sandstone [19]. In addition, the in situ direct shear test and triaxial compression test in laboratory were carried out to determine the mechanical strength of rock samples.

In situ direct shear tests were performed on the rock specimens in the pit shown in Figure 1(a). The whole testing process was carried out according to the criteria proposed by ASTM D4554-12 [14], and the field diagram of the test instrument is shown in Figure 1(b). During the test, the loading device placed horizontally can provide shear force parallel to the preset shear plane of the specimen. As shown in Figure 1(a), four specimens were designed, each with a length, width, and height of 0.6 m, 0.6 m, and 0.4 m, respectively. The test results show that the peak shear stress is inversely proportional to the normal stress. The fitting parameters of cohesion and friction angle were calculated by the linear fitting method. The final results are listed in Table 1.

Meanwhile, laboratory triaxial compression tests were carried out on the rock samples. The undisturbed rock samples were obtained by drilling holes in the test site. Three sets of samples were taken at the depth of 1.0 m, 2.0 m, and 4.0 m which are tagged as A, B, and C, respectively. The original samples were processed into cylinders of suitable size to facilitate triaxial compression tests. Finally, the shear strength index of the test samples was obtained based on the Mohr–Coulomb theory. The test results are listed in Table 2.

2.2. Foundation Installation Process. During the operation of transmission line tower foundation, due to wind and other factors, the foundation often bears the combined loads, including up-pull, down-compress, and lateral-push [20]. The uplift load has been proved to be the key design load of tower foundation [21]. Hence, as shown in Figure 2, the uplift loading test was conducted on five belled piers (named BP1~BP5) in the pilot area. The shape and symbols of the belled piers are shown in Table 3.

Similar to other field tests of cast-in-place concrete foundations [12, 13, 22, 23], the construction process of test foundations can be divided into three steps:

(1) The contour of the foundation is excavated from top to bottom slowly according to the design size. This step requires attention to the influence of groundwater. At the same time, in order to achieve the construction accuracy, dimensions are checked every 0.5 m in the process of downward excavation.

(2) The reinforcing frames of belled piers in the excavated contours are erected. The frame of the reinforcing cage is composed of vertical D28 (diameter = 28 mm) steel bar and transverse D14 (diameter = 14 mm) steel bar. The strength grade of the single steel bar is HRB335 (nominal yield stress f_y = 335 MPa). Six D64 (diameter = 64 mm) high-

Table 1: Geotechnical properties of rock samples in the field test area.

Category	G_s (kN/m^3)	w (%)	c (kPa)	φ (°)	Uniaxial saturated compressive strength of rocks R_c (MPa)
Sandstone	17.4~18.8	22.01~32.01	22.45~48.02	20.56~33.82	4.97

(a) (b)

Figure 1: In situ direct shear testing: (a) pit exploration illustration; (b) shearing test in progress.

Table 2: The results of triaxial compression tests on the rock samples in natural state.

Confining pressure (kPa)	Sample ID	Ultimate compressive strength (MPa)	Mean value (MPa)	Cohesion (MPa)	Internal friction angle (°)
	A1	1.864			
100	B1	1.754	1.623		
	C1	1.250			
	A2	2.235			
200	B2	1.961	2.023	0.407	29
	C2	1.874			
	A3	2.442			
300	B3	2.381	2.292		
	C3	2.052			

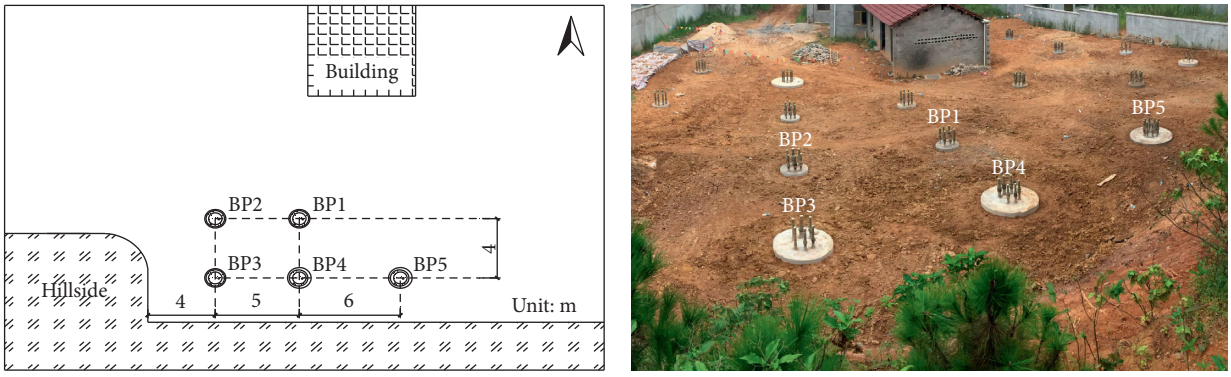

(a) (b)

Figure 2: (a) Layout chart and (b) photo indicating the arrangement of belled piers within the implementation site.

strength alloy steel anchor bolts are symmetrically arranged on the top of the foundation along a circle of 0.5 m diameter. The specified yield strength and ultimate strength of a single bolt are 930 MPa and 1,080 MPa, respectively. The length of the anchor bolt in concrete increases with the depth of foundation, and the length of the anchor bolt remained outside is 0.7 m when loading ends.

Table 3: Geometric dimensions of in situ test foundations.

	No.	d (m)	b (m)	h (m)	e (m)
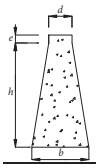	BP1	0.8	1.1	1	0.2
	BP2	0.8	1.25	1.5	0.2
	BP3	0.8	1.55	2.5	0.2
	BP4	0.8	1.7	3	0.2
	BP5	0.8	1.7	4	0.2

d is the top diameter; b is the bottom diameter; h is the embedment depth; e is the outcrop height.

(3) Pouring ready-mixed sulfate-resistant concrete into the reinforcing frames, the loading test can be carried out after 28 days of maintenance.

2.3. Field Load Test. Figure 3 shows the schematic diagram of the axial uplift loading test. As illustrated in Figure 3(b), the clear distance between the reaction concrete blocks is 10 m, which is sufficient to avoid influencing the test results. For the shaft-head displacement measurement, two electronic displacement sensors are placed symmetrically on the top of the pier along the same diameter, as shown in Figure 3(a). All the electronic displacement sensors are attached to the reference beams, as shown in Figure 3(b). The reference beams are independent from test foundation and loading device to ensure the stability of electronic displacement sensors.

The loading process was performed with static monotonic loading method without cycling, which is the typical procedure recommended by Chinese GB50007 [24]. The specific process is as follows: first, the initial load is applied at 20% of the predicted ultimate uplift load, and the incremental load per stage is half of the initial load; second, each load increment is maintained after loading until two continuous displacements are less than 0.1 mm per hour; finally, the loading process is repeated until the displacement surge occurs, at which point the foundation is considered to be completely unstable.

2.4. Test Results and Failure Criteria. Once the field tests are completed, the load-displacement curves of the five belled piers are counted as shown in Figure 4. The characteristics of these curves are similar to those of the previous tests, including belled piers under axial uplift loading in Gobi gravel or loess sloping ground [12, 13, 22, 23], micropiled raft under uplift, and compression loading in cohesive soil [25]. Similarly, the approximation of these load-displacement curves can be divided into three stages, as shown in Figure 5: (1) an initial linear stage, (2) a curvilinear transition stage, and (3) a final linear stage. With different failure criteria, the value of ultimate bearing capacity is determined at different stages.

Currently, vast amount of literature has proposed various definition and criterion of ultimate bearing capacity. Fellenius [26] defined it as a point on the load-displacement curve for which rapid displacement takes place due to a little increase in the loading. In this subsection, four common and suitable approaches have been introduced to determine the uplift capacity of test piers, including mathematical modeling method [27, 28], slope tangent method [29], tangent intersection method [30], and L_1–L_2 method [31–33]. Table 4 describes these methods and lists the corresponding values. The values determined by the mathematical modeling method and tangent intersection method can be considered as upper and lower limits of ultimate bearing capacity, respectively. The results of the slope tangent method are close, despite more conservative, to that of the L_1–L_2 method, which may lead to waste of bearing capacity of foundation. Therefore, the L_1–L_2 method is chosen as the unified failure criterion in this paper.

3. Numerical Modeling

3.1. Slope-Foundation Model. Given the goal of this paper, a numerical simulation scheme is proposed and illustrated in Figure 6. The 3D sketch of the slope-foundation model is shown in Figure 7, where a is the distance from the edge of the belled pier to the crest of the slope, d is the top diameter of the belled pier, h is the embedment depth of the belled pier, and β is the slope angle. Considering the symmetry of the current model, the half-model is chosen to improve computational efficiency. Secondly, the model of $a = 0.6$ m is selected initially, whereas the increment of a is 0.5 m each time. The criterion of stopping simulation is that the uplift bearing capacity of model n reaches the unabated performance of the belled pier far from a slope. It should be pointed out particularly that in order to obtain the unabated bearing capacity of each foundation, distance a is set as a large value in the slope-foundation model to simulate the performance of the belled pier far away from the slope. After the preliminary debugging and verification, it is determined that $a = 10$ m can meet this requirement.

3.2. Geometric Modeling. All the meshes in the simulation are established using the built in grid editor of FLAC 3D software. To set boundary conditions, the recommendations by Choi et al. [35] and Zekavati et al. [25] are considered. In this simulation, as illustrated in Figure 7, the distance from the edge of the belled pier to the surface JAEF is set to 10 m after balancing the efficiency and correctness of calculation. Considering the vertical direction of loading, the distance from the bottom of belled pier to the surface EDGF is set to 2 m. Except for the top surface JIAB and IHCB, the displacements and velocities of the nodes in each surface are fixed. In addition, several debugging calculations are carried out to eliminate the influence of meshing and boundary

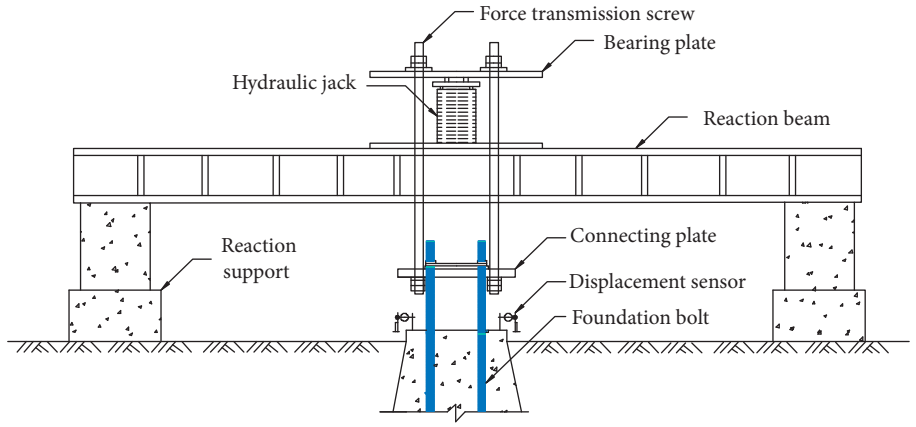

(a)

(b)

Figure 3: Schematic diagram of the axial uplift loading test: (a) schematic diagram of the loading system; (b) uplift loading test in progress.

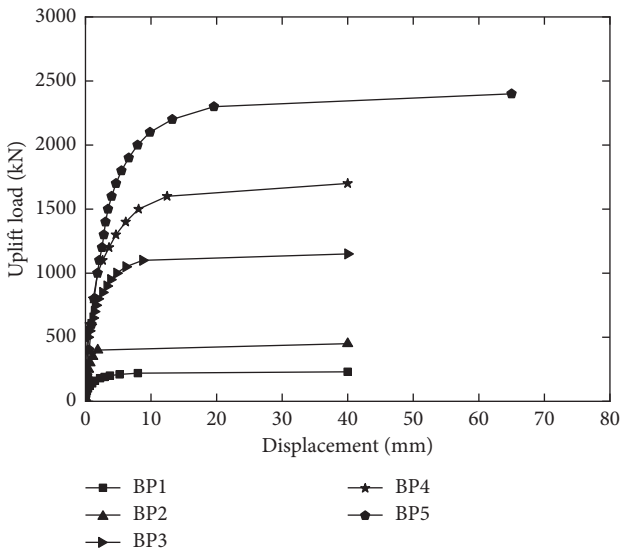

Figure 4: The uplift load-displacement curves for BP1 to BP5.

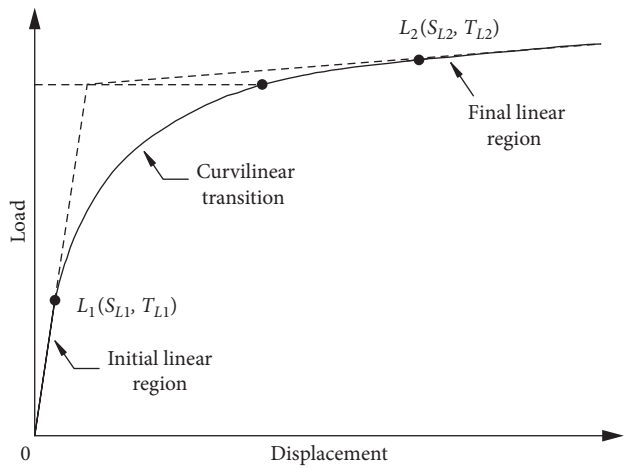

Figure 5: Sections of the load-displacement curve for the L_1–L_2 method.

Table 4: Failure criteria for determining the uplift bearing capacity of test foundations.

Method	Failure load definition	Reference	Ultimate uplift load T (kN)				
			BP1	BP2	BP3	BP4	BP5
Mathematical modeling method	For the mathematical fitting curve of the target curve, the tangent line is taken at final linear region and the tangent point is the value point	van der Veen [28] Chin [27]	230	450	1150	1700	2400
Slope tangent method	Load corresponding to the tangent point of the initial linear stage	O'Rourke and Kulhawy [29]	120	300	550	1000	1400
Tangent intersection method	Load corresponding to the tangent intersection of initial and final linear stages	Housel [30] Tomlinson [34]	200	430	1110	1480	2140
L_1–L_2 method	Load corresponding to the tangent point of the final linear stage	Hirany and Kulhawy [31–33]	230	450	1250	1600	2400

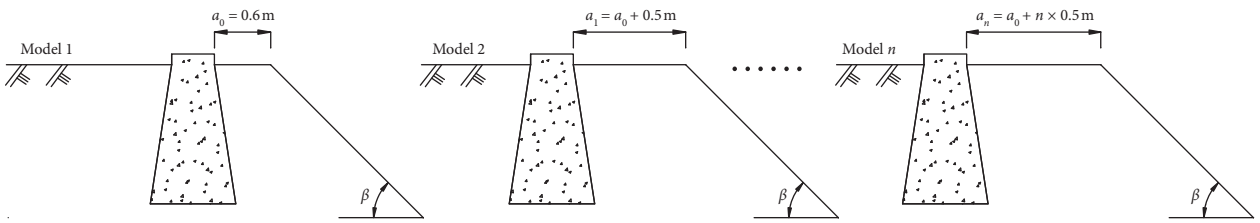

Figure 6: Flow chart of the numerical analysis scheme.

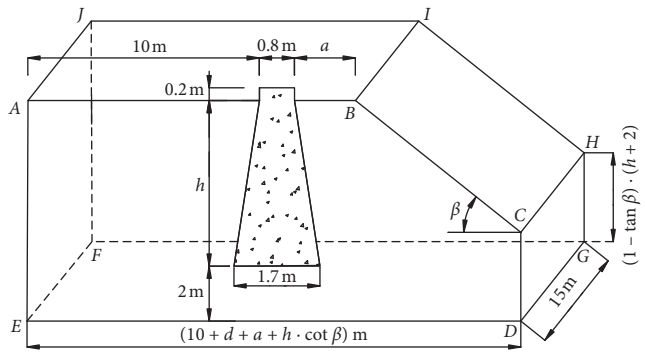

Figure 7: Geometrical dimensions of the slope-foundation model.

effect on simulation accuracy. Figure 8 depicts a 3D mesh for the slope-foundation model of $a = 2.1$ m, $h = 3$ m, and $\beta = 45°$.

3.3. Material Modeling. Material modeling involves setting up parameters of two materials, concrete and rock mass, and the interface between them. Accordingly, concrete foundation is set as linear elastic material, whereas strongly weathered rock is modeled as elastic-plastic continuous material according to the failure criterion of Mohr–Coulomb. The physical and mechanical parameters of rock and reinforced concrete are determined by in situ and laboratory tests (as listed in Tables 1 and 2). It is necessary to point out that the foundations are buried in the shallow surface with less confining pressure. Therefore, it is more reasonable to choose the results of field direct shear tests listed in Table 1 as the simulation parameters. The selected values are shown in Table 5.

The intersection of the foundation zones and the rock zones is set as "hard" contact to limit the interlacing in between and prevent tension forming along the intersection.

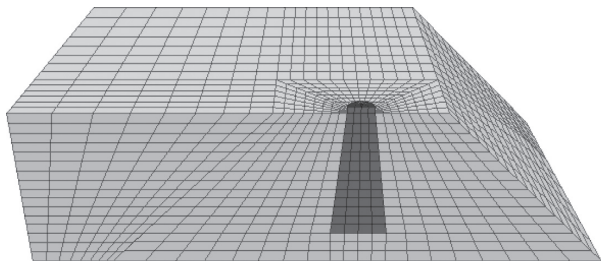

Figure 8: A 3D mesh for the half-model of $a = 2.1$ m, $h = 3$ m, and $\beta = 45^{\circ}$.

Table 5: Basic physical and mechanical parameters of rock and reinforced concrete.

Material	γ (kN/m3)	E (GPa)	Poisson's ratio	c (kPa)	φ (°)
Rock slope	18	0.34	0.3	48	25
Reinforced concrete foundation	25	30	0.2	—	—

The specific way is to set the normal stiffness (k_n) and tangential stiffness (k_s) to larger values and set them to 10 times the smaller elastic modulus of both sides according to the manual of FLAC 3D software, i.e., 3.4 GPa/m. Meanwhile, the cohesion and friction angle of the interface are set to 40 kPa and 20°, respectively.

3.4. Calibration for Slope-Foundation Model. In this section, according to the data of field tests of five belled piers, the limited aspects of the slope-foundation model are calibrated, including material parameters, model size, mesh generation, and interface parameters. The specific process is to establish five slope-foundation models with $a = 10$ m according to the size of five-field test foundations and simulate loading. The calibration criteria refer to the scheme proposed in [25], which is used to evaluate the fitting accuracy of numerical simulations and field tests of micropile. There are two criteria: (1) the coincidence of load-displacement curve and (2) the relative error of ultimate uplift load. The verification results between the field and numerical results are illustrated in Figure 9: the maximum relative error of ultimate bearing capacity is 12.5%, the minimum is 4.3%, and the average is 6.0%. The result means that the numerical simulation results of the slope-foundation model are basically consistent with the field test ones.

3.5. Simulation of Belled Piers Adjacent to Slopes. In this part, eighteen sets of slope-foundation models, which consists of three slope angles β (15°, 30°, and 45°) and six embedment depths h (3 m, 4 m, 5 m, 6 m, 8 m, and 10 m), are established and loaded. A total of 126 belled piers are simulated of loading process in corresponding models. The uplift performance of these foundations is analyzed based on the load-displacement curve and ultimate uplift capacity in the next section.

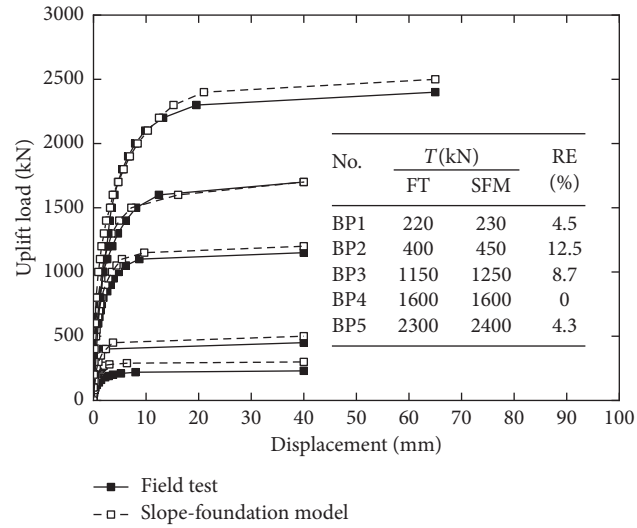

No.	T(kN) FT	T(kN) SFM	RE (%)
BP1	220	230	4.5
BP2	400	450	12.5
BP3	1150	1250	8.7
BP4	1600	1600	0
BP5	2300	2400	4.3

Figure 9: Calibration results between the numerical modeling and the field loading tests in Anhui site (RE means relative error).

3.6. Simulation Results. Figure 10 illustrates the simulation results of three groups of models, consisting of one belled pier of $h = 3$ m and three slope angles of $\beta = 15^{\circ}$, 30°, and 45°. The ultimate uplift load corresponding to each curve is obtained by the L_1–L_2 method and listed in the tables of Figure 10. For comparison, the model with $a = 10$ m is established to simulate uplift loading, whereas the ultimate uplift load is taken as the standard value, denoted by T_u. In order to quantitatively analyze the influence of slope on uplift performance of the belled pier, the concept of the attenuation coefficient is defined. The formula is as follows:

$$\omega = \frac{T_u - T_n}{T_u}, \tag{1}$$

where ω is the attenuation coefficient, T_u is the ultimate uplift load of the belled pier far away from the slopes, and T_n is the ultimate uplift load of belled pier adjacent to the slopes.

The attenuation coefficients for foundations of 3 m embedment depth with three slope angles are shown in Figure 10. The remaining fifteen sets of models are processed and analyzed in the same way. The 3D scatter plot of the variation of the attenuation coefficient ω wish respect to distance a and depth h is shown in Figure 11.

These data are analyzed qualitatively and quantitatively. First, the following observations can be made: (1) The attenuation coefficient ω is negatively correlated with the distance a and the embedment depth h, as shown in Figure 11(a), Curve I and Curve II. (2) The attenuation coefficient ω is positively correlated with the slope angle β. For example, as shown in Figures 11(a)–11(c), with the increase of angle of 15°, 30°, and 45°, the corresponding fluctuation ranges of attenuation coefficient are 0~0.02, 0~0.05, and 0~0.12, respectively. It means that the fluctuation of uplift bearing capacity of the belled pier increases along with the slope angle.

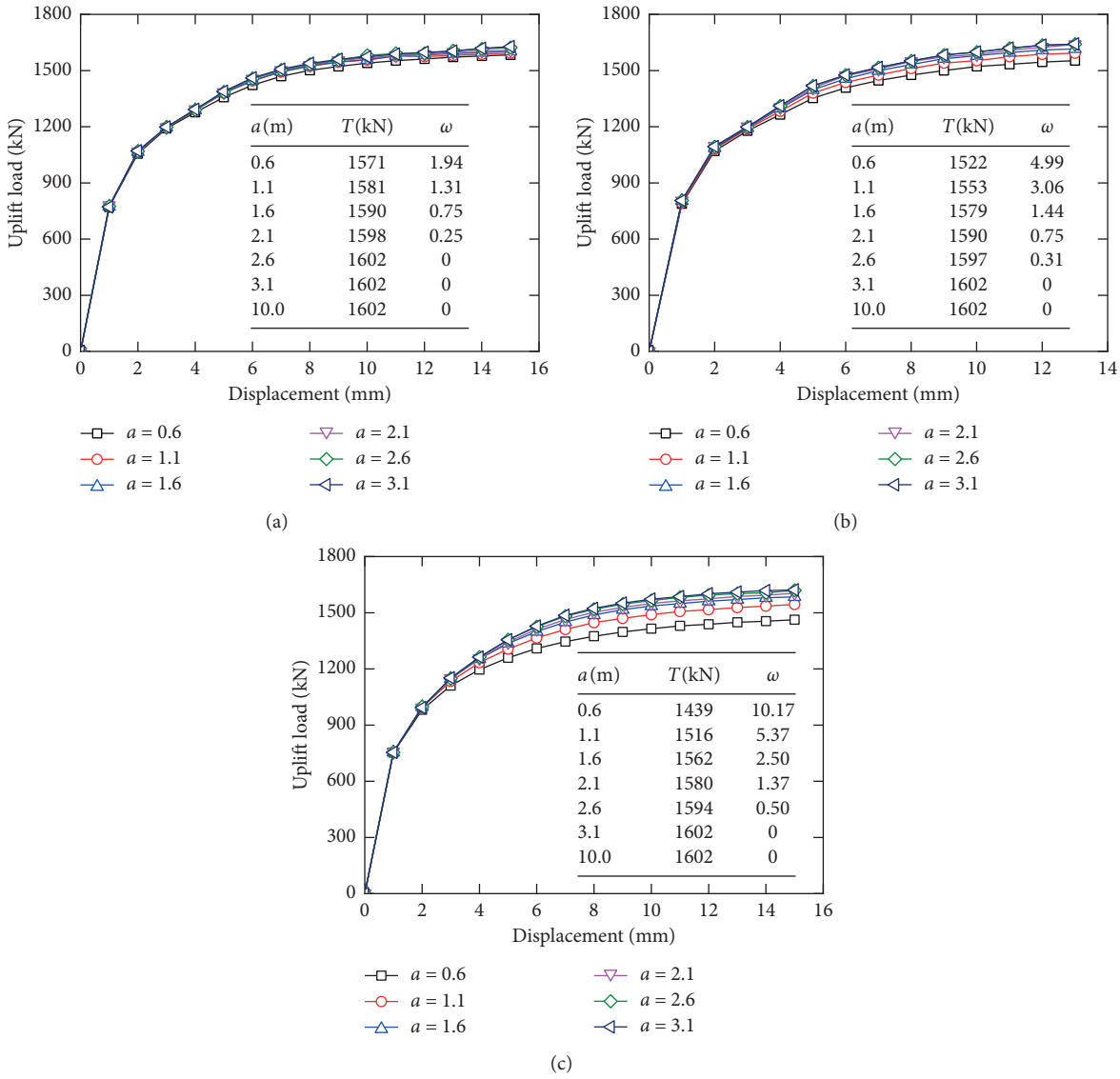

Figure 10: Simulation results of slope-foundation models with h of 3 m and β of (a) 15°, (b) 30°, and (c) 45°.

The above conclusions are consistent with common sense that (1) the closer the foundation is to the sloping ground, the shallower the embedment depth is and (2) the steeper the slope is, the more obvious the attenuation of the uplift resistance of belled pier is. These qualitative conclusions are straight forward. So it is necessary to carry out further quantitative analysis.

3.7. Analysis of Variance and F Test. In this section, based on the data in Figure 11, the influence of distance a and depth h on attenuation coefficient ω is compared by analysis of variance. By comparing the standard deviation of a and h, it can be observed which of the two factors has significant influence on the attenuation coefficient ω (the standard deviation of the main factor is greater than that of the minor factor). The calculated results are listed in Table 6. As shown in the table, the standard deviation of distance a is greater than that of embedment depth h, indicating that the former has greater influence on attenuation coefficient than the latter.

In order to test whether the difference of the influence is obvious, the joint hypothesis test (F test) is adopted. According to the process of F test, by comparing the F calculated value with the F critical value obtained by querying F table, we can determine whether the effect is significant. And as shown in Table 6, all the calculated values of F are less than the critical value of F, which means that the influence of distance a and depth h on uplift bearing capacity of belled pier is not significantly different.

3.8. Gaussian Function Fitting and Empirical Equation. After analyzing the data in Figure 11, it is considered that the data conform to the characteristics of two-dimensional Gauss distribution [36]. The surface formed by nonzero

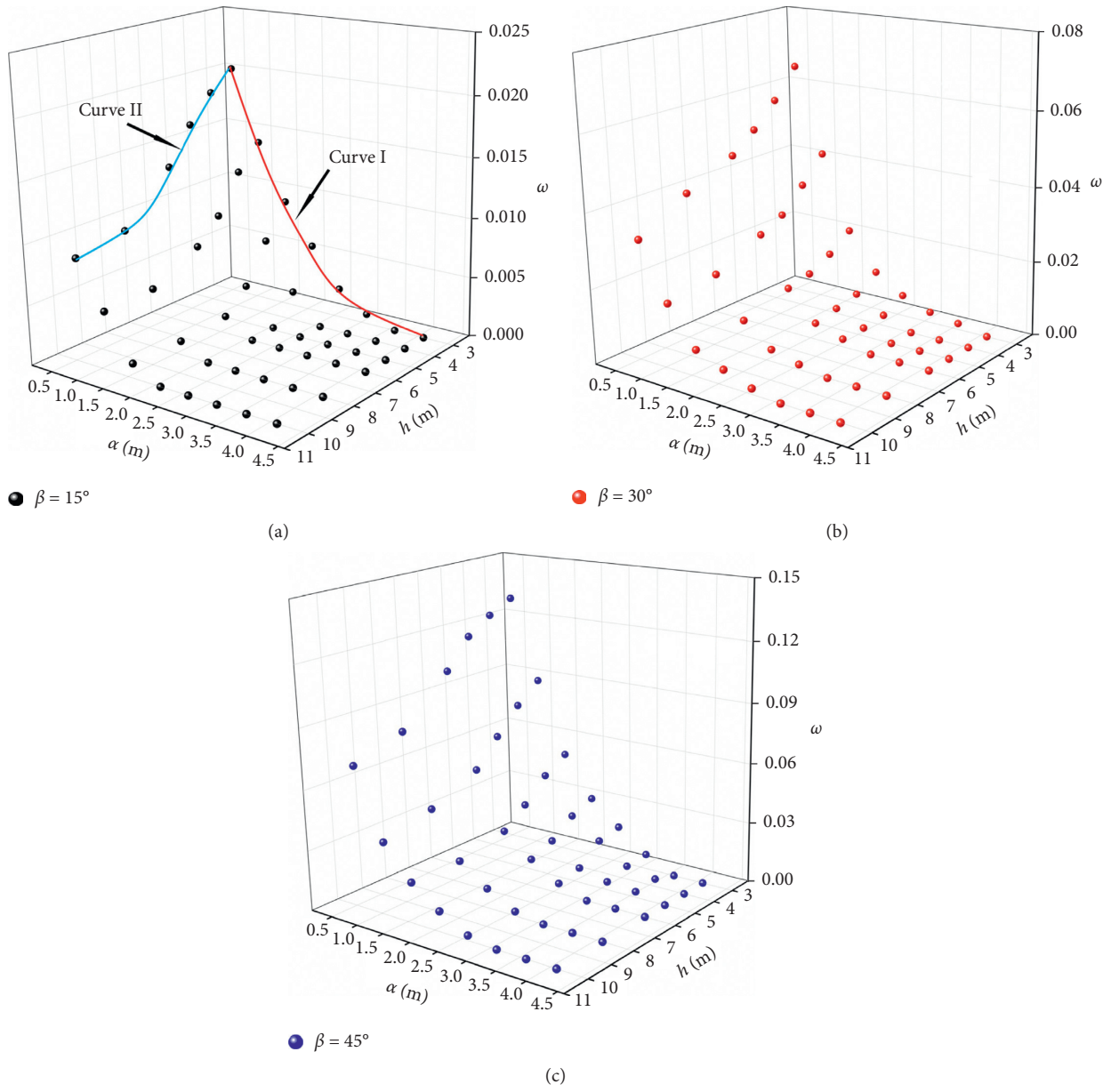

Figure 11: The 3D sketches of the attenuation coefficient ω with respect to distance a and embedment depth h with β of (a) 15°, (b) 30°, and (c) 45°.

points in Figure 11 can be approximated as a part of the surface of a two-dimensional Gauss function where the fitting equation is as follows:

$$\omega_\beta = f(a,h) = k \cdot e^{\left(-a^2/\sigma_a^2\right)} \cdot e^{\left(-h^2/\sigma_h^2\right)}, \quad (2)$$

where k is the parameter describing the range of ω_β and σ_a is the variance of distance a. In practical sense, σ_a describes the rate at which attenuation coefficient ω_β varies with distance a. σ_h is the variance of distance h. Similarly, σ_h describes the rate at which attenuation coefficient ω_β varies with depth h.

The fitted parameters are illustrated in Figure 12. The R-squared values of the results for three slope angles are 0.92, 0.97, and 0.98, respectively, which means that the fitting accuracy is high, and the choice of the Gauss function is appropriate. Furthermore, it is not difficult to find that the three fitting parameters k, σ_a, and σ_h are positively correlated with the slope angle β. Hence, the average values of these three fitting parameters were selected. The linear formulas between the fitting parameters and the slope angle β are fitted, as shown in Figure 12. The R-squared values are 0.98, 0.99, and 0.93, respectively. The empirical equation for calculating attenuation coefficient ω can be obtained by substituting the fitting parameters k, σ_a, and σ_h into equation (2), as shown in the following equation:

Table 6: The computational results of variance analysis and F test.

β (°)	Source of variance	Standard deviation	F test		
			Degree of freedom	F calculated value	F critical value
15	a	0.011	7	1.40	
	h	0.006	5		
30	a	0.123	7	1.53	4.88
	h	0.060	5		
45	a	0.574	7	1.33	
	h	0.323	5		

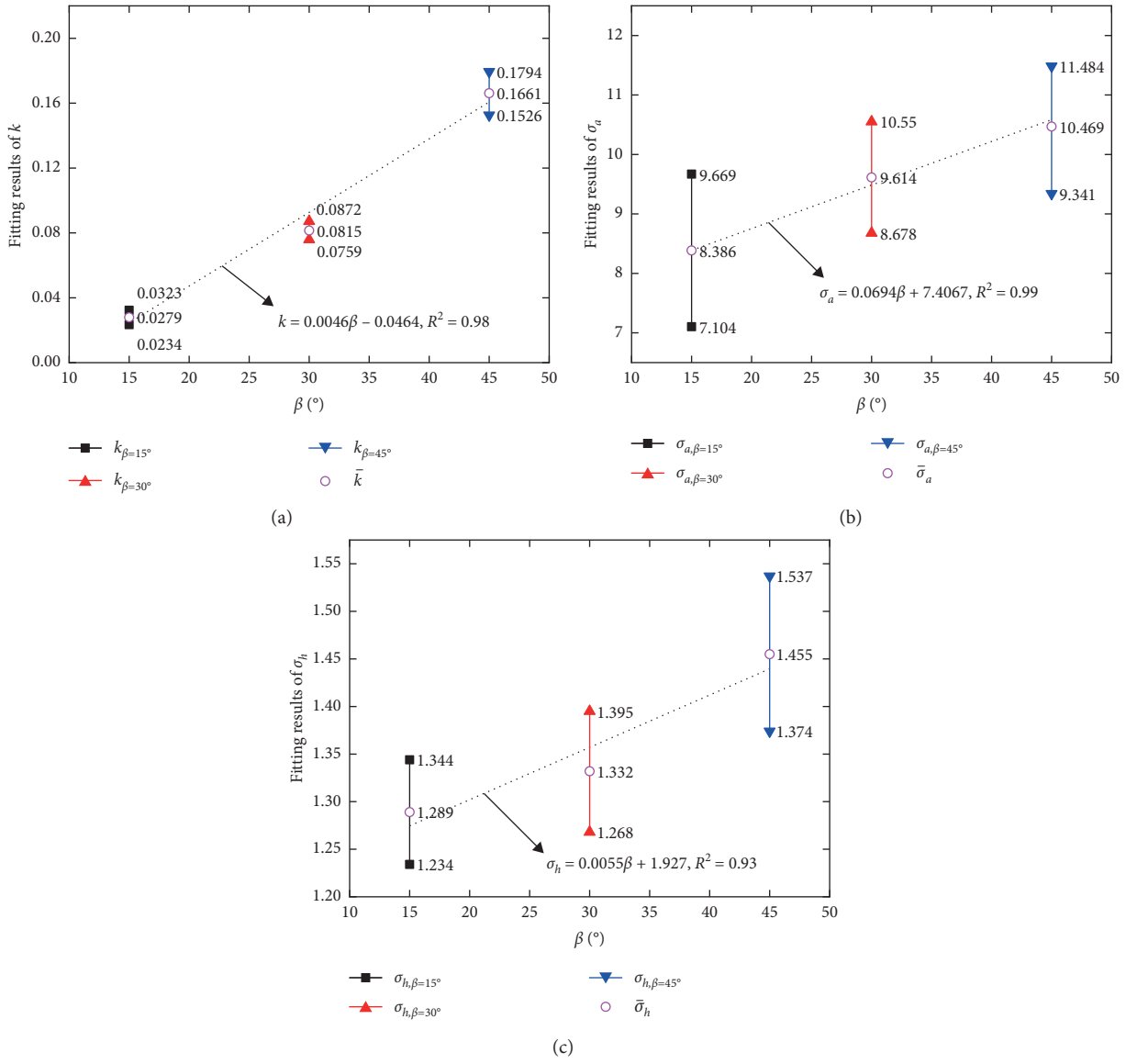

Figure 12: Fitting results of (a) k, (b) σ_a, and (c) σ_h.

$$\omega = (0.0046\beta - 0.0464) \cdot e^{-(a/0.0694\beta+7.4067)^2} \cdot e^{-(h/0.0055\beta+1.927)^2}, \quad (3)$$

where $15 \le \beta \le 45$, $0.5 \le a \le 4.1$, and $3 \le h \le 10$.

According to the actual topographic conditions in the construction process, equation (3) as a reference can be flexibly applied to the design and site selection of belled piers along the transmission line in this area.

4. Conclusions

In this research, field tests and numerical simulations are carried out on the uplift performance of belled piers

constructed in two topographical grounds. The following conclusions can be drawn:

(1) For belled piers adjacent to sloping ground, the uplift load-displacement curves can be divided into three distinct stages: initial linear stage, curvilinear transition stage, and final linear stage. These characteristics are basically consistent with that of the curves obtained from field tests of belled piers far from slopes, which indicate that the existence of slopes has no obvious effect on the shape of uplift load-displacement curves.

(2) For belled piers adjacent to the sloping ground, the attenuation coefficient ω is positively correlated with slope angle β and negatively correlated with distance a and depth h. The negative correlation between attenuation coefficient ω and distance a is stronger than that between attenuation coefficient ω and depth h. However, according to the results of F test, the difference is not significant. In the process of practical engineering, slope angle β is usually determined by the terrain. The additional distance a or the embedment depth h can increase the uplift resistance of belled pier to match the level-ground capacity. The effect of increasing the distance should be more obvious according to above the research results, which should be considered appropriately in practical designs.

(3) For belled piers adjacent to sloping ground, the empirical equation of attenuation coefficient ω determined by slope angle β, distance a, and embedment depth h is proposed based on a series of fitting results. Using this formula, the attenuation coefficient can be estimated in combination with practical engineering conditions.

(4) To summarize, in view of the uplift bearing capacity of belled piers near the sloping ground, three representative slope angles are selected for modeling study. In future work, more factors, including more slope angles, more types of foundations, and more loading directions, will be considered to improve the existing research results.

Data Availability

The source data of hundreds of numerical simulations involved in this paper are available from the corresponding author upon request.

Conflicts of Interest

The authors declare that there are no conflicts of interest regarding the publication of this paper.

Acknowledgments

This research was funded by the State Grid Corporation of China under the key scientific and technological project (GCB 17201400135).

References

[1] E. Bazán-Zurita, D. M. Williams, J. K. Bledsoe, A. D. Pugh, and F. B. Newman, "AEP 765 kV transmission line: uplift capacity of shallow foundations on sloping ground," in *Proceedings of the Electrical Transmission Line and Substation Structures: Structural Reliability in a Changing World*, pp. 215–226, Birmingham, AL, USA, October 2006.

[2] F. Castelli and V. Lentini, "Evaluation of the bearing capacity of footings on slopes," *International Journal of Physical Modelling in Geotechnics*, vol. 12, no. 3, pp. 112–118, 2012.

[3] F. Castelli and E. Motta, "Bearing capacity of strip footings near slopes," *Geotechnical and Geological Engineering*, vol. 28, no. 2, pp. 187–198, 2010.

[4] D. Chakraborty and J. Kumar, "Bearing capacity of foundations on slopes," *Geomechanics and Geoengineering*, vol. 8, no. 4, pp. 274–285, 2013.

[5] K. Georgiadis, "The influence of load inclination on the undrained bearing capacity of strip footings on slopes," *Computers Geotechnics*, vol. 37, no. 3, pp. 311–322, 2009.

[6] M. S. Keskin and M. Laman, "Model studies of bearing capacity of strip footing on sand slope," *KSCE Journal of Civil Engineering*, vol. 17, no. 4, pp. 699–711, 2013.

[7] A. Keshavarz, M. Beygi, and R. Vali, "Undrained seismic bearing capacity of strip footing placed on homogeneous and heterogeneous soil slopes by finite element limit analysis," *Computers and Geotechnics*, vol. 113, 2019.

[8] D. Raj, Y. Singh, and A. M. Kaynia, "V-H-M seismic capacity envelopes of strip foundations on slopes for capacity design of structure-foundation system," *Bulletin of Earthquake Engineering*, vol. 17, no. 6, pp. 2963–2987, 2019.

[9] Y. Xiao, M. Zhao, R. Zhang, H. Zhao, and G. Wu, "Undrained bearing capacity of strip footings placed adjacent to two-layered slopes," *International Journal of Geomechanics*, vol. 19, no. 8, 2019.

[10] F. Castelli, V. Lentini, and E. T. R. Dean, "Discussion: evaluation of the bearing capacity of footings on slopes," *International Journal of Physical Modelling in Geotechnics*, vol. 15, no. 3, pp. 165–168, 2015.

[11] C. Jiang, J.-L. He, L. Liu, and B.-W. Sun, "Effect of loading direction and slope on laterally loaded pile in sloping ground," *Advances in Civil Engineering*, vol. 2018, Article ID 7569578, 12 pages, 2018.

[12] X.-L. Lu, Z.-Z. Qian, and W.-Z. Yang, "Axial uplift behavior of belled piers in sloping ground," *Geotechnical Testing Journal*, vol. 40, no. 4, pp. 579–590, 2017.

[13] Z.-Z. Qian, X.-L. Lu, and W.-Z. Yang, "Comparative field tests on straight-sided and belled piers on sloping ground under combined uplift and lateral loads," *Journal of Geotechnical and Geoenvironmental Engineering*, vol. 145, no. 1, 2019.

[14] ASTM, *Standard Test Method for In Situ Determination of Direct Shear Strength of Rock Discontinuities*, ASTM, West Conshohocken, PA, USA, 2012.

[15] ASTM, *Standard Test Methods for Specific Gravity of Soil Solids by Water Pycnometer*, ASTM, West Conshohocken, PA, USA, 2014.

[16] ASTM, *Standard Test Method for Determination of the Point Load Strength Index of Rock and Application to Rock Strength Classifications*, ASTM, West Conshohocken, PA, USA, 2016.

[17] ASTM, *Standard Test Method for Determining Rock Quality Designation (RQD) of Rock Core*, ASTM, West Conshohocken, PA, USA, 2017.

[18] ASTM, *Standard Test Methods for Laboratory Determination of Water (Moisture) Content of Soil and Rock by Mass*, ASTM, West Conshohocken, PA, USA, 2019.

[19] CNC, "Classification and nomenclature schemes of the rocks," GB/T 17412.2-1988, National Bureau of Quality and Technical Supervision, Beijing, China, 1998, in Chinese.

[20] M. P. Pacheco, F. A. B. Danziger, and C. P. Pinto, "Design of shallow foundations under tensile loading for transmission line towers: an overview," *Engineering Geology*, vol. 101, no. 3-4, pp. 226–235, 2008.

[21] C. H. Trautmann, J. F. Beech, T. D. O'Rourke, W. McGuire, W.A. Wood, and C. Capano, "Transmission line structure foundation for uplift-compression loading," Rep. No. EPRI-EL-2870, Electric Power Research institute, Palo Alto, CA, USA, 1983.

[22] X.-L. Lu, Z.-Z. Qian, W.-F. Zheng, and W.-Z. Yang, "Characterization and uncertainty of uplift load-displacement behaviour of belled piers," *Geomechanics and Engineering*, vol. 11, no. 2, pp. 211–234, 2016.

[23] Z.-Z. Qian, X.-L. Lu, X. Han, and R.-M. Tong, "Interpretation of uplift load tests on belled piers in Gobi gravel," *Canadian Geotechnical Journal*, vol. 52, no. 7, pp. 992–998, 2015.

[24] CNC, "Code for design of building foundations," GB50007, China Architecture and Building Press, Beijing, China, 2011, in Chinese.

[25] A.-A. Zekavati, A. Khodaverdian, M.-A. Jafari, and A. Hosseini, "Investigating performance of micropiled raft in foundation of power transmission line towers in cohesive soil: experimental and numerical study," *Canadian Geotechnical Journal*, vol. 55, no. 3, pp. 312–328, 2018.

[26] B. H. Fellenius, *Basics of Foundation Design: a Geotechnical Textbook and a Background to the UniSoft Programs*, BiTech Publishers Ltd., Richmond, Canada, 1996.

[27] F. K. Chin, "Estimation of the ultimate load of piles not carried to failure," in *Proceedings of the 2nd Southeast Asian Conference on Soil Engineering*, Singapore, June 1970.

[28] C. van der Veen, "Bearing capacity of a pile," in *Proceedings of the third International Conference on Soil Mechanics and Foundation Engineering*, vol. 2, no. 3, pp. 85–90, London, UK, August 1953.

[29] T. D. O'Rourke and F. H. Kulhawy, "Observations on load tests on drilled shafts," in *Drilled Piers and Caissons II*, C. N. Baker, Ed., pp. 113–128, ASCE, Reston, VA, USA, 1985.

[30] W. S. Housel, "Pile load capacity: estimates and test results," *Journal of the Soil Mechanics and Foundations Division*, vol. 92, no. SM4, pp. 1–30, 1966.

[31] A. Hirany and F. H. Kulhawy, "Interpretation of load tests on drilled shafts. II: axial uplift," in *Proceedings of the Foundation Engineering: Current Principles and Practices*, F. H. Kulhawy, Ed., pp. 1150–1159, ASCE, Evanston, IL, USA, 1989.

[32] A. Hirany and F. H. Kulhawy, "Conduct and interpretation of load tests on drilled shaft foundations: volume 1, detailed guidelines," Final report, OSTI, Oak Ridge, TN, USA, 1988.

[33] A. Hirany and F. H. Kulhawy, "On the interpretation of drilled foundation load test results," in *Proceedings of the International Deep Foundations Congress*, Orlando, FL, USA, February 2002.

[34] M. J. Tomlinson, *Pile Design and Construction Practice (A Viewpoint Publication)*, Cement and Concrete Association of Great Britain, London, UK, 1977.

[35] Y. Choi, J. Kim, and H. Youn, "Numerical analysis of laterally loaded piles affected by bedrock depth," *Advances in Civil Engineering*, vol. 2018, Article ID 5493579, 9 pages, 2018.

[36] J. Wang and Z. Yu, "Quadratic curve and surface fitting via squared distance minimization," *Computers & Graphics*, vol. 35, no. 6, pp. 1035–1050, 2011.